Available online at www.sciencedirect.com

ScienceDirect

IFAC PapersOnline CONFERENCE PAPER ARCHIVE

IFAC PapersOnLine 56-1 (2023) 234–239

A data-driven nonlinear frequency response approach based on the Loewner framework: preliminary analysis

Ion Victor Gosea * **Luka A. Živković** **
Dimitrios S. Karachalios * **Tanja Vidaković-Koch** **
Athanasios C. Antoulas ***

* *Max Planck Institute Magdeburg, Germany, DRI group (e-mail: gosea, karachalios@mpi-magdeburg.mpg.de)*
** *Max Planck Institute Magdeburg, Germany, EEC group, (e-mail: zivkovic, vidakovic@mpi-magdeburg.mpg.de)*
*** *Electrical and Computer Engineering (ECE) Department, Rice University, Houston, Max Planck Institute, Magdeburg, Germany (DRI group) and Baylor College of Medicine, Houston, USA (e-mail: aca@rice.edu)*

Abstract: We propose a hybrid method based on the combination of computed-aided nonlinear frequency response analysis with the Loewner framework, for the characterization of nonlinear dynamical processes with application in electrochemistry. The method is data-driven, i.e., requiring only samples of the first two generalized transfer functions of the underlying system, given as values of the sampled nonlinear frequency response. Then, the established system fitting and complexity reduction approach (in the frequency domain), known as the Loewner framework, is used to extract the system's invariant quantities. In this analysis, we have used a nonlinear electrical circuit model as a test case, for which the new method provides good results.

Keywords: Data-Driven Methods, Nonlinear Dynamics, Nonlinear Frequency Response, Transfer Functions, Frequency Response Functions, Model Reduction, Non-intrusive Approach.

1. INTRODUCTION

The Nonlinear Frequency Response (NFR) is a response of a nonlinear system to a forced periodic input change with a relatively high amplitude. The system response is obtained as a sum of the first (fundamental) and higher harmonics, and a non-periodic (DC) term Petkovska (2001). Over the last two decades, a model-based Nonlinear Frequency Response method, based on the concept of higher-order frequency response functions (FRFs) was developed specifically for application in analyzing the dynamics of chemical engineering systems Petkovska (2006); Petkovska and Seidel-Morgenstern (2013); Zivkovic et al. (2020). According to the NFR method, the response of a stable weekly nonlinear system can be replaced by a set of the first-, second-, and other higher-order FRFs. More details in Petkovska and Do (2000). FRFs can be directly estimated from experimental NFR data by obtaining time and frequency-domain data of systems analyzed by periodically changing one or more system inputs. However, there are some challenges. Since mathematical derivations of the analytical solutions for FRFs can be very time-consuming and challenging, the analysis is often narrowed to analyzing simplified first principle mathematical models. To overcome this challenge, an application was made to automatize the process of obtaining FRFs. Computer-aided Nonlinear Frequency Response (cNFR) method is giving users an easy-to-use platform in which they can automatically obtain simulation-ready Matlab codes for the FRFs of the desired order Zivkovic et al. (2020). Another challenge is numerically estimating the presumed model parameters using experimental data. For this, data-based digital twin FRFs, void of noise present in measurements, could be used for the fast identification of all gains, zeros, and poles of the model-based FRFs, thus, paving the way to a new model-data-based NFR method.

Model reduction techniques can be employed to replace a system of large scale with complex structure (characterized by many differential equations), with a much simpler dynamical system (characterized by few equations with simplified structure). In the last decades, there have been many methodologies proposed in this direction; we refer the reader to Antoulas (2005); Benner et al. (2017) for more details. A viable alternative to using classical model reduction approaches (that usually require explicit access to a large-scale model), is to use instead data-driven methods such as the Loewner framework (LF). When using the latter, low-order models can be constructed directly from data. Another data-driven method that has emerged in recent years is operator inference (OpInf), which uses snapshots of the state variables, and then fits a structured nonlinear model by computing the appropriate matrices Peherstorfer and Willcox (2016); Benner et al. (2020). However, in the current contribution, the LF is more suited for connecting to the cNFR method (by using input/output data without requiring state access). Finally, we note

10.1016/j.ifacol.2023.02.040

that the LF was already applied for the identification and characterization of dynamical models for electrochemical (EC) systems in Patel et al. (2021); Sorrentino et al. (2022), but solely for purely linear analysis. The current paper presents the first application (as far as the authors know), of LF for nonlinear EC systems. In this work, the cNFR experimental and theoretical procedure for model-based analysis is combined with the data-based NFR method based on the LF proposed in Mayo and Antoulas (2007). With the newly developed NFR method, a periodically operated system can be quickly analyzed theoretically, experimentally, and combined, leading to a detailed model identification of a nonlinear system without the use of time-extensive and potentially expensive numerical integration tools. The proposed data-driven method may find applications in many branches of engineering, producing reduced-order models that can be potentially used for robust simulation, design, and control. A simple example of an electrical circuit with nonlinear components (diodes), together with resistors and capacitors was used here to test the method's performance. The paper is organized as follows; after the introduction section, we continue with Section 2 on state-space representations of (non)linear dynamical systems, derivation of FRFs, and a short description of the LF. Then, Section 3 describes the main test case of the paper, together with an exhaustive presentation of different formulations of this nonlinear system. Section 4 includes a detailed analysis of identifying the first two transfer functions of the circuit from NFR data. Finally, the conclusions and outlook are included in Section 5.

2. SOME GENERALITIES: SYSTEM THEORY, FRFS, AND THE LOEWNER FRAMEWORK

We consider linear dynamical systems characterized in the state-space realization by the system of equations:

$$\left\{\dot{\mathbf{x}}(t) = \mathbf{A}\mathbf{x}(t) + \mathbf{B}u(t), \quad y(t) = \mathbf{C}\mathbf{x}(t) \right. \quad . \tag{1}$$

where $\mathbf{x}$ is the state variable (dimension n), and system matrices are given by $\mathbf{A} \in \mathbb{R}^{n\times n}$, $\mathbf{B}, \mathbf{C}^T \in \mathbb{R}^{n\times 1}$. The transfer function of (1) is given by $H(s) = \mathbf{C}(s\mathbf{I}_n - \mathbf{A})^{-1}\mathbf{B}$, where $\mathbf{I}_n$ is a $n \times n$ identity matrix. We refer to Antoulas (2005), for more details on various methodologies especially tailored for the reduction of linear systems. In recent years, such methods for linear systems have been steadily extended to particular classes of nonlinear systems. We consider general analytical nonlinear systems characterized in state-space representation by:

$$\dot{\mathbf{x}}(t) = \mathbf{A}\mathbf{x}(t) + \mathbf{f}(\mathbf{x}(t), \mathbf{u}(t)) + \mathbf{B}u(t), \quad y(t) = \mathbf{C}\mathbf{x}(t), \tag{2}$$

where $\mathbf{f} : \mathbb{R}^n \times \mathbb{R} \to \mathbb{R}^n$ is the nonlinearity that will be approximated using Carleman's linearization in Carleman (1932), such as in Weber and Mathis (2018), or by lifting techniques from the MOR community, developed by Gu (2011) and Breiten (2013); Benner and Breiten (2015). These approaches yield a reformulated system with a polynomial (quadratic) structure (i.e., the generic nonlinearities are replaced by polynomials).

As mentioned before, data-driven approaches for the identification of reduced-order models with nonlinear dynamics typically resume to sampling the state trajectories in the time domain (and those of the derivative), such as in proper orthogonal decomposition (POD) approach Volkwein (2013), or in the OpInf methods Peherstorfer and Willcox (2016). It is to be noted that the LF has been recently extended to fit certain classes of nonlinear systems using direct numerical simulation (DNS) data, such as bilinear systems in Antoulas et al. (2016), and quadratic-bilinear (QB) systems in Gosea and Antoulas (2018). However, for these methods, data used in the computation process cannot be easily inferred from practical experiments; therefore, the motivation for developing different extensions and to propose inter-disciplinary data acquisition techniques. For the latter case, we will be concerned in this work with the cNFR method, as a tool for computing frequency-domain data (higher-order harmonic content).

2.1 Frequency response functions

The derived FRFs are present in the DC component and the first and second harmonic. In case of a co-sinusoidal change of one input (u) with the modulating amplitude A and with the forcing frequency ω, the system response consists of a sum of the DC component, the first- and higher-order harmonics:

$$y(t) = DC + h_I(t) + h_{II}(t) + \dots$$

where the non-periodic DC term of the output of interest, y, consists of the infinite number of the asymmetrical FRFs of the even-order:

$$\begin{aligned} DC \approx\ & 2\left(\frac{A}{2}\right)^2 G_2(\omega, -\omega) \\ & + 6\left(\frac{A}{2}\right)^4 G_4(\omega, \omega, -\omega, -\omega) + \dots \end{aligned}$$

The DC term corresponds to the non-periodic and nonlinear part of the response and can be used to estimate the mean output value of a system whose inputs are periodically modulated, as shown in Petkovska and Seidel-Morgenstern (2013).

The first harmonic, $h_I(t)$, can be estimated with the first- and higher-odd-order FRFs:

$$\begin{aligned} h_I(t) \approx\ & \left(\frac{A}{2}\right)\left(e^{j\omega t}G_1(\omega) + e^{-j\omega t}G_1(-\omega)\right) \\ & + 3\left(\frac{A}{2}\right)^3\left(e^{j\omega t}G_3(\omega, \omega, -\omega) + e^{-j\omega t}G_3(\omega, -\omega, -\omega)\right) + \dots \end{aligned}$$

The first harmonic contains linear information about the system response when the forcing amplitudes are sufficiently small. Therefore, the first-order FRFs can be used for mechanism identification in linear systems.

The second harmonic, $h_{II}(t)$, can be estimated with the second and other even-order symmetrical FRFs:

$$\begin{aligned} h_{II}(t) \approx\ & \left(\frac{A}{2}\right)^2\left(e^{j2\omega t}G_2(\omega, \omega) + e^{-j2\omega t}G_2(-\omega, -\omega)\right) \\ & + 4\left(\frac{A}{2}\right)^4\left(e^{j2\omega t}G_4(\omega, \omega, \omega, -\omega) + e^{-j2\omega t}G_4(\omega, -\omega, -\omega, -\omega)\right) \\ & + \dots \end{aligned}$$

Since the second harmonic contains most of the system's nonlinearity information, it can be used to identify systems in cases where the first harmonic does not have enough discrimination potential, as shown in Zivkovic et al. (2020).

2.2 The Loewner framework for linear systems

For the case of linear systems in (1), the starting point for the LF is to collect measurements corresponding to the

(first) transfer function, which can be inferred in practice from the first harmonic. The data are first partitioned into two disjoint subsets:

$$\begin{aligned} &\text{right data}: (\lambda_j; w_j),\ j = 1, \ldots, k, \text{ and,} \\ &\text{left data}: (\mu_i; v_i),\ i = 1, \ldots, k, \end{aligned} \tag{3}$$

find the rational function $\tilde{H}(s)$, such that the following interpolation conditions are (approximately) fulfilled:

$$\tilde{H}(\mu_i) = v_i, \quad \tilde{H}(\lambda_j) = w_j. \tag{4}$$

The Loewner matrix $\mathbb{L} \in \mathbb{C}^{k\times k}$ and the shifted Loewner matrix $\mathbb{L}_s \in \mathbb{C}^{k\times k}$ are defined as follows

$$\mathbb{L}_{(i,j)} = \frac{v_i - w_j}{\mu_i - \lambda_j},\ \mathbb{L}_{s(i,j)} = \frac{\mu_i v_i - \lambda_j w_j}{\mu_i - \lambda_j}, \tag{5}$$

while the data vectors $\mathbb{V}, \mathbb{W}^T \in \mathbb{R}^k$ are introduced as

$$\mathbb{V}_{(i)} = v_i, \quad \mathbb{W}_{(j)} = w_j, \text{ for } i, j = 1, \ldots, k. \tag{6}$$

The Loewner model is hence constructed as follows:

$$\mathbf{E} = -\mathbb{L}, \quad \mathbf{A} = -\mathbb{L}_s, \quad \mathbf{B} = \mathbb{V}, \quad \mathbf{C} = \mathbb{W}.$$

Provided that enough data is available, the pencil $(\mathbb{L}_s, \mathbb{L})$ is often singular. In these cases, a singular value decomposition (SVD) of augmented Loewner matrices is computed, in order to find projection matrices $\mathbf{X}_r, \mathbf{Y}_r \in \mathbb{C}^{k\times r}$, as described in Antoulas et al. (2017). Here, $r < n$ represents the truncation index. Then, the system matrices corresponding to a projected Loewner model of dimension r (here, $(\cdot)^*$ denotes the conjugate-transpose) can be computed using the truncated matrices $\mathbf{X}_r$ and $\mathbf{Y}_r$, as:

$$\hat{\mathbf{E}} = -\mathbf{X}_r^* \mathbb{L} \mathbf{Y}_r, \quad \hat{\mathbf{A}} = -\mathbf{X}_r^* \mathbb{L}_s \mathbf{Y}_r, \quad \hat{\mathbf{B}} = \mathbf{X}_r^* \mathbb{V}, \quad \hat{\mathbf{C}} = \mathbb{W}\mathbf{Y}_r,$$

and therefore, directly finds a state-space realization corresponding to the reduced-order system of equations

$$\left\{ \hat{\mathbf{E}}\dot{\hat{\mathbf{x}}}(t) = \hat{\mathbf{A}}\mathbf{x}(t) + \hat{\mathbf{B}}u(t), \quad \hat{y}(t) = \hat{\mathbf{C}}\hat{\mathbf{x}}(t). \right. \quad . \tag{7}$$

The transfer function of the reduced Loewner model in (7) is written as $\hat{H}(s) = \hat{\mathbf{C}}(s\hat{\mathbf{E}} - \hat{\mathbf{A}})^{-1}\hat{\mathbf{B}}$, and it provides an accurate fit to the original transfer function $H(s)$. Then, $\hat{H}(s)$ may be expanded in a pole/zero, pole/residue, or a time-constant/gain format (for the latter, see Patel et al. (2021)). These values represent the system invariants, that can be related to the circuit blocks. It is noted that the state-space realization is not unique, and that is why an extra step is required. More implementation details and properties of the LF procedure can be found in Antoulas et al. (2017); Karachalios et al. (2021a).

3. THE TEST-CASE: A NON-LINEAR CIRCUIT

We consider the nonlinear electrical circuit in Fig. 3. Each

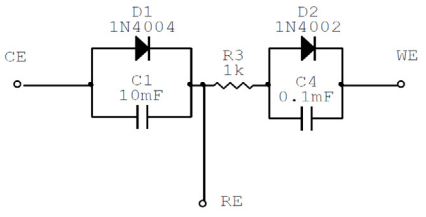

Fig. 1. A schematic of the nonlinear circuit.

block contains a capacitor in parallel with a diode. This is modeled as a dynamical system in two variables given by the voltage drops on each block. Similar electrical circuits, but with linear elements (e.g., a simple resistor instead of a diode), are routinely used in electrochemical (EC) laboratories to test devices. They resemble the behavior of an EC interface. In the present case, a diode mimics a nonlinearity of an EC reaction. Therefore, the abbreviations in Fig. 3 correspond to typical abbreviations in an EC 3-electrode cell where: RE is the "reference electrode", WE the "working electrode", and CE the "counter electrode". In general, EC experiments are performed with either current or potential as input. In the present case, it was chosen that the current is the input, while the output is the potential difference between CE and WE. The observed output is the sum of the potential losses ($V_1(t)$ and $V_2(t)$) at two elements mimicking the *two electrodes* of an EC cell and potential loss on resistor R_3, mimicking the *Ohmic loss* in the electrolyte/membrane. More precisely, we can write the differential equations characterizing the dynamics as:

$$\begin{cases} C_1 \dfrac{dV_1(t)}{dt} = I(t) - I_{r_1}\left(e^{\frac{1}{V_{t_1}}V_1(t)} - 1\right), \\ C_4 \dfrac{dV_2(t)}{dt} = I(t) - I_{r_2}\left(e^{\frac{1}{V_{t_2}}V_2(t)} - 1\right), \end{cases} \tag{8}$$

while the observed output is given by

$$y(t) = V_1(t) + V_2(t) + R_3 I(t).$$

The capacitance values are denoted with $C_i, 1 \le i \le 2$, while other constants are denoted with I_{r_i} and V_{t_i}. Next, we introduce the following notations: $x_1(t) = V_1(t)/V_{t_1},\ x_2(t) = V_2(t)/V_{t_2}$, and let

$$a = \frac{1}{C_1 V_{t_1}},\ b = \frac{1}{C_4 V_{t_2}},\ c = I_{r_1},\ d = I_{r_2}. \tag{9}$$

Using all of these new variables, the nonlinear system in (8) is rewritten as:

$$\begin{cases} \dot{x}_1(t) = aI(t) - ac\left(e^{x_1(t)} - 1\right), \\ \dot{x}_2(t) = bI(t) - bd\left(e^{x_2(t)} - 1\right), \\ y(t) = V_{t_1}x_1(t) + V_{t_2}x_2(t) + R_3 I(t). \end{cases} \tag{10}$$

3.1 Analysis based on Taylor series truncation

The methods discussed in this section are inexact, i.e., they are based on approximation by truncating the Taylor series associated with the nonlinearity. In some practical scenarios, such approaches provide a good enough solution. First, by using a truncated Taylor series (around 0) given by the formula $e^{x_i(t)} \approx 1 + x_i(t)$, and substitute it in (10), it remains the following linear dynamical system:

$$\begin{cases} \dot{x}_1(t) = aI(t) - acx_1(t), \\ \dot{x}_2(t) = bI(t) - bdx_2(t), \\ y(t) = x_1(t)V_{t_1} + x_2(t)V_{t_2} + R_3 I(t). \end{cases} \tag{11}$$

Then, identify the following linear realization:

$$\mathbf{A}_L = \begin{bmatrix} -ac & 0 \\ 0 & -bd \end{bmatrix},\ \mathbf{B}_L = \begin{bmatrix} a \\ b \end{bmatrix},\ \mathbf{C}_L = \begin{bmatrix} V_{t_1} & V_{t_2} \end{bmatrix},\ \mathbf{D}_L = R_3$$

Next, we will also present Carleman's linearization, originally proposed in Carleman (1932). It is a method used to embed a nonlinear system of differential equations of finite dimension into a system of bilinear differential equations of infinite dimension. However, truncation is often performed. We introduce the new state variable $\mathbf{x}^C$ as

$$\mathbf{x}^C = \begin{bmatrix} \mathbf{x} \\ \mathbf{x} \otimes \mathbf{x} \end{bmatrix} = \begin{bmatrix} x_1 & x_2 & x_1^2 & x_1x_2 & x_2x_1 & x_2^2 \end{bmatrix}^T, \tag{12}$$

and we explicitly compute the derivatives of the last four entries of $\mathbf{x}^C$. By neglecting higher-order polynomial terms, an approximated bilinear system is derived as:

$$\begin{cases} \dot{x}^C(t) \approx \mathbf{A}_C\mathbf{x}^C(t) + \mathbf{N}_C\mathbf{x}^C(t)u(t) + \mathbf{B}_C u(t), \\ y(t) \quad = \mathbf{C}_C\mathbf{x}^C(t) + \mathbf{D}_C u(t). \end{cases}$$

3.2 Exact lifting

It is to be mentioned that all reformulations shown so far are based on *approximating* the original dynamics, and hence, they are *not exact*. In what follows, we show an *exact* reformulation, that is not based on truncating or neglecting any terms; it is based on lifting. The first step towards implementing a lifting approach is to identify the quantities that depend non-linearly on the original states. For example, we define auxiliary variables as:

$$x_3(t) := e^{x_1(t)} - 1, \quad x_4(t) := e^{x_2(t)} - 1. \tag{13}$$

Remark 3.1. Note that zero initial conditions are hence enforced, provided that the original two variables $x_1(t)$ and $x_2(t)$, start also at zero (i.e., $x_1(0) = x_2(0) \Rightarrow x_3(0) = x_4(0) = \mathbf{0}$). If these conditions are not a priori satisfied, one needs to define new state variables as:

$$\tilde{x}_1(t) = x_1(t) - x_1(0), \quad \tilde{x}_2(t) = x_2(t) - x_2(0), \tag{14}$$

where $x_1(0) = V_1(0)/V_{t_1}$ and $x_2(0) = V_2(0)/V_{t_2}$.

In the particular case considered above (zero initial conditions), the new system is written as:

$$\begin{cases} \dot{x}_1(t) = aI(t) - acx_3(t), \quad \dot{x}_2(t) = bI(t) - bdx_4(t), \\ \dot{x}_3(t) = -acx_3(t) - acx_3^2(t) + aI(t) + ax_3(t)I(t) \\ \dot{x}_4(t) = -bdx_4(t) - bdx_4^2(t) + bI(t) + bx_4(t)I(t) \\ \quad y(t) = x_1(t)V_{t_1} + x_2(t)V_{t_2} + R_3I(t). \end{cases}$$

The dynamical system above can be written in a standard quadratic-bilinear format, as follows:

$$\begin{cases} \dot{\mathbf{x}}(t) = \mathbf{A}\mathbf{x}(t) + \mathbf{Q}(\mathbf{x}(t) \otimes \mathbf{x}(t)) + \mathbf{N}\mathbf{x}(t)u(t) + \mathbf{B}u(t), \\ y(t) = \mathbf{C}\mathbf{x}(t) + \mathbf{D}u(t), \end{cases} \tag{15}$$

where the newly augmented state variable is given by:

$$\mathbf{x}(t) = [x_1(t)\ x_2(t)\ x_3(t)\ x_4(t)]^T \in \mathbb{R}^{4\times 1}, \tag{16}$$

and the system matrices of the lifted system are defined:

$$\mathbf{A} = \begin{bmatrix} 0 & 0 & -ac & 0 \\ 0 & 0 & 0 & -bd \\ 0 & 0 & -ac & 0 \\ 0 & 0 & 0 & -bd \end{bmatrix}, \mathbf{N} = \begin{bmatrix} 0 & 0 & 0 & 0 \\ 0 & 0 & 0 & 0 \\ 0 & 0 & a & 0 \\ 0 & 0 & 0 & b \end{bmatrix}, \ \mathbf{B} = \begin{bmatrix} a \\ b \\ a \\ b \end{bmatrix}, \ \mathbf{D} = R_3,$$

$$\mathbf{C} = \begin{bmatrix} V_{t_1} \\ V_{t_2} \\ 0 \\ 0 \end{bmatrix}^T, \mathbf{Q} = \begin{bmatrix} 0 & 0 & 0 & 0 & 0 & 0 & 0 & 0 & 0 & 0 & 0 & 0 & 0 & 0 & 0 & 0 \\ 0 & 0 & 0 & 0 & 0 & 0 & 0 & 0 & 0 & 0 & 0 & 0 & 0 & 0 & 0 & 0 \\ 0 & 0 & 0 & 0 & 0 & 0 & 0 & 0 & 0 & 0 & 0 & 0 & -ac & 0 & 0 & 0 \\ 0 & 0 & 0 & 0 & 0 & 0 & 0 & 0 & 0 & 0 & 0 & 0 & 0 & 0 & 0 & -bd \end{bmatrix}.$$

The first two symmetric transfer functions of the QB system in (15) can be written explicitly in terms of the system's matrices, as shown previously in Gu (2011); Benner and Breiten (2015) and in subsequent publications. Hence, by using those explicit formulas, we can compute the first two transfer functions (evaluated at the same frequency value s). These are expressed in terms of s, but also in terms of the parameters of the circuit, as follows:

$$\begin{aligned} G_1(s) &= \mathbf{C}\mathbf{\Phi}(s)\mathbf{B} = \frac{V_{t_1}}{C_1V_{t_1}s + I_{r_1}} + \frac{V_{t_2}}{C_4V_{t_2}s + I_{r_2}} + R_3, \\ G_2(s,s) &= \mathbf{C}\mathbf{\Phi}(2s)\mathbf{Q}\left[\mathbf{\Phi}(s)\mathbf{B} \otimes \mathbf{\Phi}(s)\mathbf{B}\right] + \mathbf{C}\mathbf{\Phi}(2s)\mathbf{N}\mathbf{\Phi}(s)\mathbf{B} \\ &= \frac{I_{r_1}V_{t_1}}{2\left(I_{r_1} + C_1\,V_{t_1}\,s\right)^2\left(I_{r_1} + 2\,C_1\,V_{t_1}\,s\right)} \\ &\quad + \frac{I_{r_2}V_{t_2}}{2\left(I_{r_2} + C_2\,V_{t_2}\,s\right)^2\left(I_{r_2} + 2\,C_2\,V_{t_2}\,s\right)} \end{aligned} \tag{17}$$

Here, we have used the notation: $\mathbf{\Phi}(s) = (s\mathbf{I}_4 - \mathbf{A})^{-1}$. In general, explicit formulations of the transfer functions in terms of the system's matrices (operators) as in (17) can be directly derived only for polynomial systems. The parameters can be recovered from the LF by considering the 2nd kernel as a univariate rational function. Similar studies have been proposed in Karachalios et al. (2021b); Gosea et al. (2021) for inferring bilinear or quadratic systems respectively.

4. THE PROPOSED ANALYSIS ON THE CIRCUIT

4.1 Theoretical analysis

The first transfer function in (17), can explicitly be represented in pole-residue representation as

$$G_1(s) = R_3 + \frac{\frac{1}{C_1}}{s - \left(-\frac{I_{r_1}}{C_1V_{t_1}}\right)} + \frac{\frac{1}{C_4}}{s - \left(-\frac{I_{r_2}}{C_4V_{t_2}}\right)} \tag{18}$$

Hence, the first transfer function $G_1(s)$ can be expressed as a sum of two rational fractions of the first order plus a constant term. This suggests, as correctly identified by the Loewner framework in the next section, that the order of the underlying linear model that explains $G_1(s)$ is $r_1 = 2$ (R_3 is the feed-through term).

The poles and residues can hence be expressed in terms of the circuit elements as:

(1) residues: $\gamma_i = \frac{1}{C_i}$ (2) poles: $\pi_i = -\frac{I_{r_i}}{C_iV_{t_i}}$, $1 \le i \le 2$;

The formulation of $G_2(s,s)$ in (17) can be simplified accordingly, and hence the second order TF is given by

$$\begin{aligned} G_2(s,s) &= \frac{I_{r_1}/(2C_1)}{(2s + I_{r_1}/(C_1V_{t_1}))\,(s + I_{r_1}/(C_1V_{t_1}))^2} \\ &\quad + \frac{I_{r_2}/(2C_2)}{(2s + I_{r_2}/(C_2V_{t_2}))\,(s + I_{r_2}/(C_2V_{t_2}))^2} \\ &= \frac{I_{r_1}/(2C_1)}{(2s+\pi_1)(s+\pi_1)^2} + \frac{I_{r_2}/(2C_2)}{(2s+\pi_2)(s+\pi_2)^2} \\ &= \frac{I_{r_1}\gamma_1}{(s+\pi_1/2)(s+\pi_1)^2} + \frac{I_{r_2}\gamma_2}{(s+\pi_2/2)(s+\pi_2)^2} \end{aligned} \tag{19}$$

By using the partial fraction formula below:

$$\frac{\gamma}{(s+\alpha)(s+\beta)^2} = \frac{A}{s+\alpha} + \frac{B}{s+\beta} + \frac{\Gamma}{(s+\beta)^2}, \tag{20}$$

where $A = -\frac{\gamma}{(\alpha-\beta)^2}$, $B = \frac{\gamma}{(\alpha-\beta)^2}$, $\Gamma = \frac{\gamma}{\alpha-\beta}$, we obtain that $G_2(s,s)$ can be written as:

$$\begin{aligned} G_2(s,s) &= \frac{I_{r_1}\gamma_1}{(s+\pi_1/2)(s+\pi_1)^2} + \frac{I_{r_2}\gamma_2}{(s+\pi_2/2)(s+\pi_2)^2} \\ &= \frac{-\frac{4I_{r_1}\gamma_1}{\pi_1^2}}{s+\pi_1} + \frac{\frac{4I_{r_1}\gamma_1}{\pi_1^2}}{s+\pi_1/2} + \frac{\frac{2I_{r_1}\gamma_1}{\pi_1}}{(s+\pi_1/2)^2} + \frac{-\frac{4I_{r_2}\gamma_2}{\pi_2^2}}{s+\pi_2} \\ &\quad + \frac{\frac{4I_{r_2}\gamma_2}{\pi_2^2}}{s+\pi_2/2} + \frac{\frac{2I_{r_2}\gamma_2}{\pi_2}}{(s+\pi_2/2)^2}. \end{aligned} \tag{21}$$

Hence, the second (uni-variate) transfer function $G_2(s,s)$ can be expressed as a sum of four rational fractions of the first order plus two rational fractions of the second order. This suggests, as correctly identified by the Loewner framework in the next section, that the order of the underlying linear model that explains $G_2(s)$ is $r_2 = 6$.

Remark 4.1. By applying the Loewner approach to samples of $G_1(s)$, we recover the corresponding poles and residues/zeros of the rational function $G_1(s)$. Then, one is able to recover the capacitance values as well as the ratios between the diode coefficients, but not the individual coefficients themselves:

$$C_i = \frac{1}{\gamma_i}, \ \frac{I_{r_i}}{V_{t_i}} = -\frac{\pi_i}{\gamma_i}, \ 1 \le i \le 2. \tag{22}$$

This illustrates the fact that information from the linear block (using data from $G_1(s)$ only) is not enough for a correct characterization of the circuit; an extended analysis of $G_2(s,s)$ is hence needed.

4.2 Loewner analysis on the nonlinear circuit

Analysis for $G_1(s)$ Next, we consider as data, samples of the uni-variate function $G_1(s)$ on a frequency grid $2\pi[10^{-6}, 10^{2}]$j (200 logarithmically-spaced points). We hence fit a linear model using the Loewner approach; the transfer function of this fitted model is written as:

$$\hat{G}_1^{\mathrm{L}}(s) = \frac{\hat{\kappa}^{(1)}(s-\hat{\zeta}_1^{(1)})(s-\hat{\zeta}_2^{(1)})}{(s-\hat{\pi}_1^{(1)})(s-\hat{\pi}_2^{(1)})}. \tag{23}$$

The exact values computed by means of the Loewner framework, that account for the representation of $\hat{G}_1^{\mathrm{L}}(s)$ above, are explicitly given in Tab. 1.

Poles	Zeros	Gain
$\hat{\pi}_1^{(1)} = -147.0590$	$\hat{\zeta}_1^{(1)} = -154.5256$	$\hat{\kappa}^{(1)} = 985.5000$
$\hat{\pi}_2^{(1)} = -2.1932$	$\hat{\zeta}_2^{(1)} = -2.2990$	

Table 1. The poles, zeros and gain identified with the Loewner procedure ($\hat{G}_1^{\mathrm{L}}(s)$)

As illustrated by the decay of the singular values (SVs) corresponding to the Loewner matrices in Fig. 2 (magenta circles for $\mathbb{L}$, i.e., the Loewner matrix, and green squares for $\mathbb{L}_s$, i.e., the shifted Loewner matrix), there is a shift of one SV encountered that suggests the presence of a feed-through term (given here by R_3); for more details on this phenomenon, see Antoulas et al. (2017).

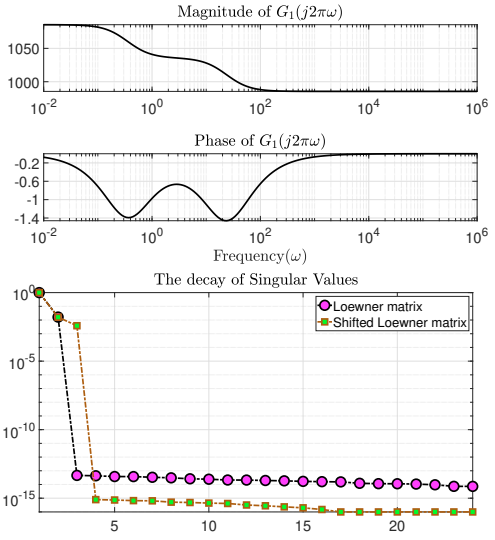

Fig. 2. Magnitude and phase of $G_1(s)$ (up); the singular value decay of the Loewner matrices (down).

The correct order $r_1 = 2$ is predicted by the SV decay of the Loewner matrix (the third singular value of $\mathbb{L}$ is close to 0). This shows the power of the LF approach, since it provides an a priori estimate of the system's order. Finally, the Loewner fitted model is compared (in the frequency domain) to the original data, provided by the cNFR method. The results are shown in Fig. 3. A good agreement is observed especially in the low frequency range (between $2\pi 10^{-2}$ and $2\pi 10^{2}$). For the higher frequency range, we notice an increasing miss-match (although, still reasonably low), which can be explained by the constant polynomial term (Ohmic resistance) R_3, which characterizes the behavior at infinity.

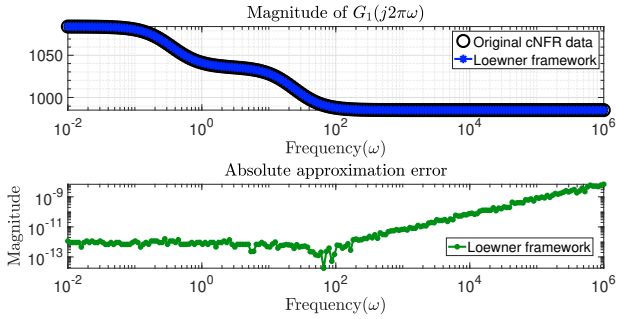

Fig. 3. Original cNFR data and the LF (up); the absolute approximation error achieved by LF (down).

Analysis for $G_2(s,s)$ Next, we consider as given data, a collection of samples of the uni-variate function $G_2(s,s)$ evaluated on the same frequency grid as for $G_1(s)$, i.e., 200 sampling points in $2\pi[10^{-6}, 10^{2}]$j. We fit a linear model using the Loewner approach; the transfer function of this model is hence written as:

$$\hat{G}_2^{\mathrm{L}}(s) = \tag{24}$$
$$= \frac{\hat{\kappa}^{(2)}(s-\hat{\zeta}_1^{(2)})(s-\hat{\zeta}_2)(s-\hat{\zeta}_3^{(2)})}{(s-\hat{\pi}_1^{(2)})(s-\hat{\pi}_2^{(2)})(s-\hat{\pi}_3^{(2)})(s-\hat{\pi}_4^{(2)})(s-\hat{\pi}_5^{(2)})(s-\hat{\pi}_6^{(2)})}.$$

The exact values identified through LF, that enter the above formulation of $\hat{G}_2^{\mathrm{L}}(s)$, are provided in Tab. 2.

Poles	Zeros
$\hat{\pi}_1^{(2)} = -147.0590 + \epsilon$j	$\hat{\zeta}_1^{(2)} = -0.9520 + 1.4284$j
$\hat{\pi}_2^{(2)} = -147.0590 - \epsilon$j	$\hat{\zeta}_2^{(2)} = -0.9521 - 1.4284$j
$\hat{\pi}_3^{(2)} = -73.5294$	$\hat{\zeta}_3^{(2)} = -3.5801$
$\hat{\pi}_4^{(2)} = -2.1932$	Gain
$\hat{\pi}_5^{(2)} = -2.1932$	$\hat{\kappa}^{(2)} = 3.9754 \cdot 10^{10}$
$\hat{\pi}_6^{(2)} = -1.0967$	

Table 2. The poles, zeros and gain values identified with the Loewner approach for $\hat{G}_2^{\mathrm{L}}(s)$.

In the above table, the value for ϵ is quite small and explicitly given by $3.6358 \cdot 10^{-5}$. This perturbation can be explained as a direct influence of the Jordan blocks in the Loewner pencil (i.e., producing numerical inaccuracies).

Again, as it can be clearly observed by the SV decay presented in Fig. 4, the LF approach again correctly identifies the order of the underlying rational function. Additionally, as predicted by the theory, the poles of $\hat{G}_2^{\mathrm{L}}(s)$ are doubled copies of the poles of $\hat{G}_1^{\mathrm{L}}(s)$ (4 values), together with the halved poles (2 values). Finally, the frequency response of the Loewner fitted model is compared to the original data, provided by the cNFR method. A good agreement is observed in Fig. 5, especially in the high frequency range (between $2\pi 10^4$ and $2\pi 10^6$). This is explained by the fact that the rational function fitted here is strictly proper, i.e., $\lim_{s\to\infty} G2(s,s) = 0$.

5. CONCLUSIONS AND OUTLOOK

In this work, a hybrid identification method was introduced. This is based on combining a recently proposed

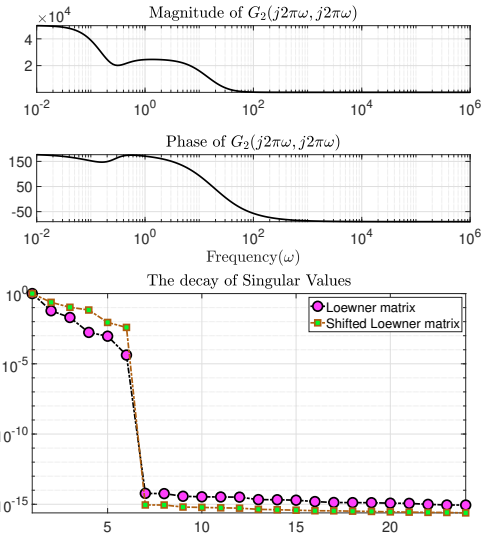

Fig. 4. Magnitude and phase of $G_2(s, s)$ (up); the singular value decay of the Loewner matrices (down).

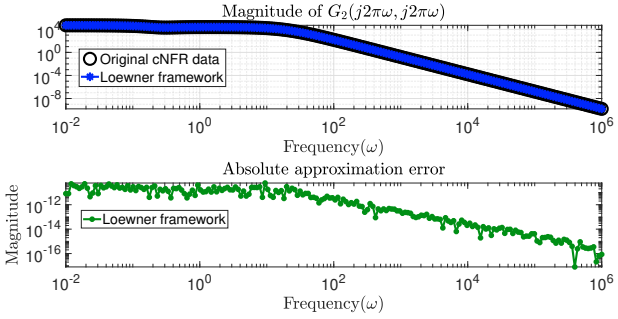

Fig. 5. Original cNFR data and the LF fit (up); the absolute approximation error achieved by LF (down).

automated nonlinear frequency response analysis (cNFR) with already an established data-driven modeling approach, i.e., the Loewner framework. The main application is the characterization of nonlinear dynamical processes in electrochemistry. The method is data driven, i.e., since it needs only input/output data as samples of transfer functions of the underlying system; these are given in a practical context as values of the nonlinear frequency response. The Loewner framework is then used to extract system-invariant components. In this preliminary analysis, we have used a nonlinear electrical circuit model as a test case. Further research endeavors will consist in applying the method for noisy/perturbed data (measured in the laboratory), and in providing quadratic-bilinear or general polynomial extensions of the Loewner framework for identifying more complicated and diverse EC systems.

REFERENCES

Antoulas, A.C. (2005). *Approximation of large-scale dynamical systems*. SIAM, Philadelphia.

Antoulas, A.C., Gosea, I.V., and Ionita, A.C. (2016). Model reduction of bilinear systems in the Loewner framework. *SIAM Journal on Scientific Computing*, 38(5), B889–B916.

Antoulas, A.C., Lefteriu, S., and Ionita, A.C. (2017). A tutorial introduction to the Loewner framework for model reduction. In *Model Reduction and Approximation*, chapter 8, 335–376. SIAM.

Benner, P. and Breiten, T. (2015). Two-sided projection methods for nonlinear model order reduction. *SIAM Journal on Scientific Computing*, 37(2), B239–B260.

Benner, P., Goyal, P., Kramer, B., Peherstorfer, B., and Willcox, K. (2020). Operator inference for non-intrusive model reduction of systems with non-polynomial nonlinear terms. *Comp. Methods in App. Mechanics and Engineering*, 372.

Benner, P., Ohlberger, M., Cohen, A., and Willcox, K. (2017). *Model Reduction and Approximation*. Society for Industrial and Applied Mathematics, Philadelphia, PA.

Breiten, T. (2013). *Interpolatory Methods for Model Reduction of Large-Scale Dynamical Systems*. Dissertation, Dep. of Mathematics, Otto-von-Guericke University, Magdeburg, Germany.

Carleman, T. (1932). Application de la théories des équations intégrales linéaires aux systèmes d'équations différentielles non linéaires. *Acta. Math.*, 59, 63–87.

Gosea, I.V. and Antoulas, A.C. (2018). Data-driven model order reduction of quadratic-bilinear systems. *Numerical Linear Algebra with Applications*, 25(6), e2200.

Gosea, I.V., Karachalios, D.S., and Antoulas, A.C. (2021). Learning reduced-order models of quadratic dynamical systems from input-output data. In *2021 European Control Conference*, 1426–1431.

Gu, C. (2011). A projection-based nonlinear model order reduction approach using quadratic-linear representation of nonlinear systems. *IEEE Transactions on Computer-Aided Design of Integrated Circuits and Systems*, 30(9), 1307–1320.

Karachalios, D.S., Gosea, I.V., and Antoulas, A.C. (2021a). The Loewner framework for system identification and reduction. In P. Benner and et al. (eds.), *Model Reduction Handbook: Volume I: System- and Data-Driven Methods and Algorithms*, Handbook on Model Reduction, 181–228. De Gruyter.

Karachalios, D.S., Gosea, I.V., and Antoulas, A.C. (2021b). On bilinear time-domain identification and reduction in the Loewner framework. In *Model Reduction of Complex Dynamical Systems*, volume 171 of *International Series of Numerical Mathematics*, 3–30. Birkhäuser, Cham. doi:10.1007/978-3-030-72983-7_1.

Mayo, A.J. and Antoulas, A.C. (2007). A framework for the solution of the generalized realization problem. *Linear Algebra and Its Applications*, 425(2-3), 634–662.

Patel, B., Sorrentino, A., Gosea, I.V., Antoulas, A., and Vidakovic-Koch, T. (2021). Application of Loewner framework for data-driven modeling and interpretation of impedance spectra of polymer electrolyte membrane fuel cells. *Proceedings EFCF*, 295–304.

Peherstorfer, B. and Willcox, K. (2016). Data-driven operator inference for nonintrusive projection-based model reduction. *Computer Methods in Applied Mechanics and Engineering*, 306, 196–215.

Petkovska, M. (2001). Nonlinear frequency response of nonisothermal adsorption systems. *Nonlinear Dynamics*, 26, 351–370.

Petkovska, M. and Seidel-Morgenstern, A. (2013). Evaluation of periodic processes in periodic operation of reactors, by P.L. Silveston and R.R. Hudgins (editors), Bitherworth. 387–413.

Petkovska, M. (2006). Nonlinear frequency response method for investigation of equilibria and kinetics of adsorption systems. *Surfactant science series*, 130, 283–327.

Petkovska, M. and Do, D.D. (2000). Use of higher-order frequency response functions for identification of nonlinear adsorption kinetics: Single mechanisms under isothermal conditions. *Nonlinear Dynamics*, 21(4), 353–376.

Sorrentino, A., Gosea, I.V., Patel, B., Antoulas, A.C., and Vidakovic-Koch, T. (2022). Loewner framework and distribution of relaxation times of electrochemical systems: Solving issues through a data-driven modeling approach. *Available at SSRN (Social Science Research Network), 4217752*.

Volkwein, S. (2013). Proper orthogonal decomposition: Theory and reduced-order modelling. *Lecture Notes, Konstanz*, 4(4), 1–29.

Weber, H. and Mathis, W. (2018). Analysis and design of nonlinear circuits with a self-consistent carleman linearization. *IEEE Trans. on Circuits and Systems I: Regular Papers*, 65(12), 4272–4284.

Zivkovic, L.A., Vidakovic-Koch, T., and Petkovska, M. (2020). Computer-aided nonlinear frequency response method for investigating the dynamics of chemical engineering systems. *Processes*, 8(11), 1354.